Masked inverse folding with sequence transfer for protein representation learning

Kevin K. Yang
Microsoft Research
yang.kevin@microsoft.com

Niccolò Zanichelli
EleutherAI
niccolo.zanichelli@gmail.com

Hugh Yeh
University of Chicago
hughy@uchicago.edu

Abstract

Self-supervised pretraining on protein sequences has led to state-of-the art performance on protein function and fitness prediction. However, sequence-only methods ignore the rich information contained in experimental and predicted protein structures. Meanwhile, inverse folding methods reconstruct a protein's amino-acid sequence given its structure, but do not take advantage of sequences that do not have known structures. In this study, we train a masked inverse folding protein language model parameterized as a structured graph neural network. We then show that using the outputs from a pretrained sequence-only protein masked language model as input to the inverse folding model further improves pretraining perplexity. We evaluate both of these models on downstream protein engineering tasks and analyze the effect of using information from experimental or predicted structures on performance.

1 Introduction

Large pretrained protein language models (MLMs) have advanced the ability of machine-learning methods to predict protein structure, function, and fitness from sequence, especially when labeled training data is sparse. The recent state-of-the-art, inspired by BERT ((bidirectional encoder representations from transformers) [Devlin et al., 2018], uses increasingly-large transformer [Vaswani et al., 2017] models to reconstruct masked and mutated protein sequences taken from databases such as UniProt [UniProt Consortium, 2021], UniRef [Suzek et al., 2015], and BFD [Steinegger et al., 2019, Steinegger and Söding, 2018]. Pretrained protein MLMs contain structural information [Rao et al., 2019, Rives et al., 2021, Chowdhury et al., 2021], encode evolutionary trajectories [Hie et al., 2022a, 2021], are zero-shot predictors of mutation fitness effects [Meier et al., 2021], improve out-of-domain generalization on protein engineering datasets [Dallago et al., 2021], and suggest improved sequences for engineering [Hie et al., 2022b]. Protein MLMs are now incorporated into the latest machine-learning methods for detecting signal peptides [Teufel et al., 2021] and predicting intracellular localization[Thumuluri et al., 2022]. However, only training on sequences ignores the rich information contained in experimental and predicted protein structures, especially as the number of high-quality structures from AlphaFold [Jumper et al., 2021, Varadi et al., 2022] increases.

Meanwhile, inverse folding methods reconstruct a protein's amino-acid sequence given its structure. Deep learning-based inverse folding is usually parametrized as a graph neural network (GNN) [Ingraham et al., 2019, Strokach et al., 2020, Jin et al., 2021, Jing et al., 2020] or SE(3)-equivariant transformer [McPartlon et al., 2022] that either reconstructs or autoregressively decodes the amino-acid sequence conditioned on the desired backbone structure. The ability to generate amino-acid

sequences that fold into a desired structure is useful for developing novel therapeutics [Chevalier et al., 2017], biosensors [Quijano-Rubio et al., 2021], industrial enzymes [Siegel et al., 2010], and targeted small molecules [Lucas and Kortemme, 2020]. Furthermore, single-chain inverse folding approaches could be coupled with recent sequential assembly based multimer structure prediction techniques [Bryant et al., 2022] for fixed-backbone multimer design.

However, we are primarily interested in using inverse folding as a pretraining task, with the intuition that incorporating structural information should improve performance on downstream tasks. Furthermore, current inverse folding methods must be trained on sequences with known or predicted structures, and thus do not take maximal advantage of the large amount of sequences that do not have known structures or of the menagerie of pretrained protein MLMs. For example, UniRef50 contains 42 million sequences, while the PDB [Rose et al., 2016]. currently contains 190 thousand experimentally-measured protein structures.

In this study, we train a **M**asked **I**nverse **F**olding (MIF) protein masked language model (MLM) parameterized as a structured graph neural network (SGNN) [Ingraham et al., 2019]. We then show that using the outputs from a pretrained sequence-only protein MLM as input to MIF further improves pretraining perplexity. We will refer to this model as **M**asked **I**nverse **F**olding with **S**equence **T**ransfer (MIF-ST). Figure 1 compares our previous sequence-only dilated convolutional protein MLM (CARP), MIF, and MIF-ST. We evaluate MIF and MIF-ST on downstream protein engineering tasks and analyze the effect of experimental and predicted structures on performance. Finally, we comment on the state of pretrained models for protein fitness prediction.
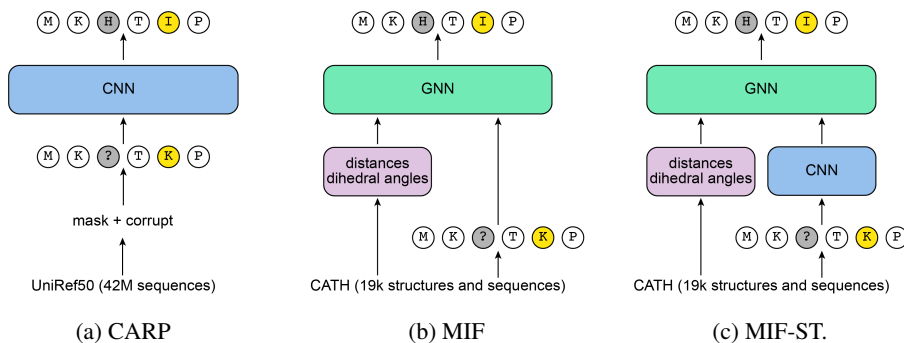
2 MIF and MIF-ST

Figure 1: Summary of models: (a) the **C**onvolutional **A**utoencoding **R**epresentations of **P**roteins protein masked language model, (b) the **M**asked **I**nverse **F**olding model, and (c) the **M**asked **I**nverse **F**olding with **S**equence **T**ransfer model.

2.1 Background

Proteins are chains of amino acids that fold into three-dimensional structures. In masked language modeling pretraining on protein sequences, a model learns to reconstruct the original protein sequence from a corrupted version, and then the model likelihoods are used to make zero-shot predictions or the pretrained weights are used as a starting point for training on a downstream task, such as structure or fitness prediction. For example, ESM [Rives et al., 2021] and CARP [Anonymous, 2022] use the corruption scheme first described in BERT [Devlin et al., 2018]. With a vocabulary of $\mathbb{T}$ of amino acids, we start from an amino-acid sequence s of length L of amino acids $s_i \in \mathbb{T} : 1 \leq i \leq L$, 15% of positions $\mathbb{M}$ are selected uniformly at random. 80% of these are changed to a special mask token, 10% are randomly mutated to another amino acid, and the remaining 10% are unchanged to generate s_{noised}. The model learns to predict the original amino acids:

$$p\left(s_i | s_{\text{noised}}\right) \forall i \in \mathbb{M} \tag{1}$$

by minimizing the negative log likelihood at positions $i \in \mathbb{M}$.

2

2.2 Masked inverse folding

While MLM pretraining on protein sequences can encode structural and functional information, adding information about the protein's backbone structure improves sequence recovery. A protein's backbone structure consists of the coordinates for each amino-acid residue's C, C_α, C_β, and N atoms, leaving out information about the side chains (which would trivially reveal each residue's amino-acid identity). We call the pretraining task of reconstructing a corrupted protein sequence conditioned on its backbone structure **M**asked **I**nverse **F**olding, which is illustrated in Figure 1b. We use the BERT corruption scheme and train the model to reconstruct the original amino acids conditioned on the corrupted sequence and the backbone structure:

$$p\left(\boldsymbol{s}_i | \boldsymbol{s}_{\text{noised}}, \text{structure}\right) \forall i \in \mathbb{M} \tag{2}$$

After pretraining, a MIF model can be used to perform any downstream task that a sequence-only PMLM can, with the caveat that a structure must be provided. Intuitively, structure-conditioned pretraining and having access to structures for the downstream task should both improve performance. We now discuss masked inverse folding in detail.

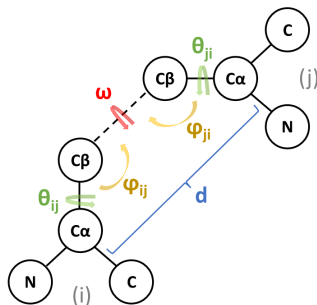### 2.2.1 Embedding backbone structure and sequence

Figure 2: The backbone atoms amino-acid residues i and j with their dihedral and planar angles highlighted.

We represent protein backbone structures as graphs $\mathcal{G} = (\mathcal{V}, \mathcal{E})$ where each node $\mathcal{V}$ is an amino acid connected by edges $\mathcal{E}$ to its k-nearest amino-acid neighbors in the structure. We set $k = 30$ throughout. Each node's structural input features consist of the sine and cosine transformations of its dihedral and planar angles to its nearest neighbors in the primary structure:

$$\mathcal{V}_i = \{\sin, \cos\} \times \{\omega_{i,i+1}, \phi_{i+1,i}, \phi_{i,i+1}, \psi_{i+1,i}, \psi_{i,i+1}\} \in \mathbb{R}^{10} \tag{3}$$

Note that ω coordinates are symmetric whereas ϕ and ψ coordinates are asymmetric and depend on residue order, so we encode both the forward and backwards angles in the forward and backward direction, i.e. $\phi_{i+1,i}$, and $\phi_{i,i+1}$, respectively. Figure 2 illustrates the backbone atoms of two residues and shows their dihedral and planar angles.

The input edge features for the ith residue consist of the dihedral and planar angles and the Euclidean distance $d_{i,j\in N(i,k)}$ between the C_α atom of residue i and the C_α atoms of its k-nearest neighbors, $N(i,k)$:

$$\mathcal{E}_i = \{d_{i,j}\} + \{\sin, \cos\} \times \{\omega_{i,j}, \phi_{i,j}, \phi_{j,i}, \psi_{i,j}, \psi_{j,i}\} \in \mathbb{R}^{k \times 11} \tag{4}$$

where $j \in N(i,k)$ and $j \neq i$.

We embed each token in $\boldsymbol{s}$ into a vector of size d_s:

$$\boldsymbol{S} = \text{embed}\left(\boldsymbol{s}\right) \in \mathbb{R}^{L \times d_s} \tag{5}$$

and concatenate it to the structural input node features to arrive at:

3

$$V = \text{concat}\,(\mathcal{V}, \boldsymbol{S}) \in \mathbb{R}^{L \times (10+d_s)} \tag{6}$$

Finally, we embed each edge and node into the model dimension d:

$$\boldsymbol{V}^0 = \boldsymbol{W}_v \boldsymbol{V} + \boldsymbol{b}_v \in \mathbb{R}^{L \times d} \tag{7}$$

$$\boldsymbol{E}^0 = \boldsymbol{W}_e \mathcal{E} + \boldsymbol{b}_e \in \mathbb{R}^{L \times k \times d} \tag{8}$$

Throughout, we set $d = 256$ and $d_s = 30$.

2.2.2 Structured GNN

We parametrize MIF as a bidirectional version of the structured GNN from Ingraham et al. [2019]. The node and edge embeddings $\boldsymbol{V}^0$ and $\boldsymbol{E}^0$ are passed to a standard message-passing GNN with a multilayer perceptron aggregation function. The mth GNN layer takes as input node representations $\boldsymbol{V}^{m-1}$ and edge representations $\boldsymbol{E}^{m-1}$ and outputs $\boldsymbol{V}^m$ and $\boldsymbol{E}^m$. Within each layer, we first gather relational information from every neighboring node

$$R_i^m = \text{concat}\left(E_{j \in N(i,k)}^{m-1}, V_{j \in N(i,k)}^{m-1}\right) \in \mathbb{R}^{k \times 2d} \tag{9}$$

and then compute the incoming messages at each node:

$$h_i^m = \text{Agg}\left[f_{msg}(R_i^{(m)})\right] \in \mathbb{R}^d \tag{10}$$

We parameterize f_{msg} as a three layer neural network with hidden dimension d and ReLU non-linearities and Agg as a mean over the neighbor dimension. We then compute new node embeddings with another feed-forward neural network.

$$V_i^m = f_{\text{update}}\left(V_i^{m-1}, h_i^m\right) \tag{11}$$

The sequence logits are computed as a linear mapping of the final node representations.

2.2.3 Datasets and model training

We trained a 4-layer MIF on the CATH4.2 dataset Sillitoe et al. [2019] using the training, validation, and testing splits from Ingraham et al. [2019], in which there is no overlap between CATH topology classifications between data splits. MIF was trained with dynamic batch sizes to maximize GPU utilization with a maximum batch size of 6000 tokens or 100 sequences, the Adam optimizer, a maximum learning rate of 0.001, and a linear warmup over 1000 steps. Models were trained on one Nvidia V100 GPU for approximately one day, until validation perplexity stopped improving.

Previously, we trained CARP-640M, a dilated convolutional protein masked language model with approximately 640 million parameters trained on UniRef50 that achieves comparable results to the state-of-the-art transformer protein MLM, ESM-1b, which has a similar number of parameters and is trained on an earlier release of UniRef50. Importantly, all sequences with greater than 30% identity to the CATH test set were removed from CARP-640M's training set in order to obtain a fair evaluation on the CATH test set. As shown in Table 1, conditioning on the backbone structure drastically improves perplexity and sequence recovery compared to CARP-640M, despite MIF having 20 times fewer parameters and being trained on only the 19 thousand examples in CATH compared to the 42 million sequences in UniRef50. Increasing the GNN depth to 8 layers does not improve pretraining performance, so we use MIF with 4 layers for all following experiments.

2.3 Masked Inverse Folding with Sequence Transfer

While conditioning on structure improves sequence recovery compared to sequence-only pretraining, we hypothesized that transferring information from sequences for which no structure is available should further improve performance on the pretraining task. Therefore, we transfer sequence information from CARP-640M by directly replacing the sequence embedding in Equation 5 with the

Table 1: Pretrained models. Parameters is the number of parameters trained on CATH4.2. Perplexity and recovery are on the CATH4.2 test set from [Ingraham et al., 2019].

Regime	Model	Parameters	Perplexity	Recovery
sequence only	CARP-640M	640M	7.06	40.5%
sequence & structure	MIF-4	3.4M	4.95	49.9%
	MIF-8	6.8M	5.00	46.7%
+sequence transfer	MIF-ST	3.4M	4.08	55.6%
-UniRef50 pretraining	MIF-ST	3.4M	5.70	45.4%

outputs from CARP-640M pretrained on UniRef50, as shown in Figure 1c. MIF-ST was trained with identical hyperparameters to MIF. The pretrained CARP-640M weights were not finetuned during training on CATH4.2. As shown in Table 1, sequence transfer improves perplexity and recovery on the CATH4.2 test set over both CARP-640M and MIF. Using the CARP-640M architecture with randomly-initialized weights as input to MIF did not improve performance, showing simply increasing model capacity is insufficient and that sequence transfer is necessary for the improvement.

3 Related Work

Sequence-only protein language models A large body of work has recently studied the application of language models to sequence-only protein generation [Madani et al., 2020, 2021, Shin et al., 2021, Ferruz et al., 2022, Hesslow et al., 2022] and representation learning. See Wu et al. [2021] for a more comprehensive review of *de novo* protein sequence design with deep generative models. Alley et al. [2019] demonstrate that the internal representation learned by an LSTM-based autoregressive protein language model trained on a large protein sequence dataset can be leveraged for a wide variety of downstream tasks, including stability, fluorescence and secondary structure prediction. Rives et al. [2021], Rao et al. [2019, 2020], Elnaggar et al. [2021], Brandes et al. [2021] improve upon this by using the transformer architecture Vaswani et al. [2017], replacing the autoregressive pretraining task with a bidirectional denoising task, and scaling up the model and dataset sizes. Rao et al. [2021] further extend protein language models by allowing it to attend to multiple sequence alignments. [Anonymous, 2022] replace the transformer attention module with dilated convolutions. MIF and MIF-ST build on this body of work by combining the denoising task with structural conditioning.

Fixed-backbone protein design This is similar in spirit to work in fixed-backbone protein design, which involves the design of proteins with a given target backbone structure. Outside of deep-learning based methods, researchers use packing algorithms [Dahiyat and Mayo, 1997, Street and Mayo, 1999, DeGrado et al., 1991, Harbury et al., 1998], physics-based energy functions [Alford et al., 2017], or match structural motifs to sequence motifs [Zhou et al., 2020]. More recent methods attempt to invert deep-learning protein structure prediction models [Jendrusch et al., 2021, Moffat et al., 2021, 2022, Anishchenko et al., 2021, Norn et al., 2021, Wang et al., 2021]. See Ovchinnikov and Huang [2021] for a more comprehensive review of fixed-backbone protein design approaches.

Our method is most similar to work that directly conditions sequence generation on an encoding of the backbone structure. Ingraham et al. [2019] conditions an autoregressive sequence model on inter-residue distances and angles. Although Ingraham et al. [2019] focuses on a Structured Transformer, they note that replacing the transformer attention mechanism with a simple multilayer perceptron improves performance, and we use this Structured GNN architecture in both MIF and MIF-ST. Jing et al. [2020] improves on the results in Ingraham et al. [2019] by modeling all the backbone coordinates with a new geometric vector perceptron (GVP) architecture. McPartlon et al. [2022] replaces GVP with an SE(3)-equivariant transformer. MIF-ST uses sequence transfer via a sequence masked language model to improve MIF. Similarly, Strokach et al. [2020] augments experimental structures by assuming that sequence homologs will fold to the same structure, while Hsu et al. [2022] augments GVP with 12 million structures predicted by AlphaFold2. In contrast to these methods, our focus is on learning sequence from structure as a pretraining task instead of as the primary design task, and we therefore train a bidirectional denoising model instead of an autoregressive language model.

5

Representations of protein structure While we condition on structure and reconstruct sequence, there are other methods for incorporating protein structural information, such as predicting structure similarity between protein sequences [Bepler and Berger, 2019], corrupting and reconstructing the structure in addition to the sequence [Mansoor et al., 2021, Chen et al., 2022], encoding surface features [Townshend et al., 2019], contrastive learning [Zhang et al., 2022, Cao et al., 2021], or a graph encoder without sequence decoding [Somnath et al., 2021, Fuchs et al., 2020]. LM-GVP uses the same architecture as MIF-ST consisting of a pretrained language model feeding into a GNN that encodes backbone structure [Wang et al., 2022]. However, in LM-GVP the structure-aware module is used as a finetuned prediction head without any pretraining.

4 Downstream tasks

We evaluate MIF and MIF-ST on downstream tasks relevant to protein engineering, including zero-shot mutation effect prediction and out-of-domain generalization.

4.1 Zero-shot mutation effect prediction

Large language models can predict experimental measurements of protein function without further training on sequence-fitness measurements or sets of evolutionarily-related sequences Hie et al. [2022a], Meier et al. [2021]. Table 2 reports results on the following datasets:

1. DeepSequence: 41 deep mutational scanning datasets originally compiled by Riesselman et al. [2018]. These datasets each measure the effects of thousands of mutations or combinations of mutations to a parent sequence. Models are evaluated on their average Spearman ρ across the datasets. We ensemble results from five AlphaFold structures obtained using ColabFold [Mirdita et al., 2021] default parameters for each wild-type protein.

2. Mutation Stability Prediction (MSP): Townshend et al. [2021] curate single mutants from SKEMPI [Jankauskaite et al., 2018], which measures whether mutant proteins display better binding than wildtype. Models are evaluated using area under the receiver operating curve (AUROC) on the 893 positive and 3255 negative examples in the test set.

3. Stability: Rocklin et al. [2017] used deep mutational scans to measure protease stability for point mutants of a set of *de novo* designed miniproteins with 10 different folds. Models are evaluated on their average Pearson correlation across the folds.

4. RBD: Starr et al. [2020] performed a deep mutational scan to measure how all amino-acid mutations to the receptor binding domain (RBD) of the SARS-CoV-2 spike protein affected its affinity to the human ACE2 receptor. Models are thus tasked to predict binding affinity for all 1311 mutant RBD sequences. We use PDB 6M0J as the native structure.

5. GB1: Wu et al. [2016] performed a 4-site combinatorial deep mutational scan on protein G domain B1, an immunoglobulin-binding protein expressed in Streptococcal bacteria. Models are evaluated on Spearman ρ across all measurements using an AlphaFold structure of the 56-amino acid GB1 domain.

We score sequences by masking every mutated position and computing the log odds ratio between the mutated and wild-type residues at each mutated position, assuming an additive model when a sequence contains multiple mutations (the "masked marginal" method from Meier et al. [2021]) except for stability, where we use the pseudolikelihood. Where possible, we compare to ESM-1v, which is an ensemble of five masked language models trained on UniRef90, Structured Transformer, the SE(3)-equivariant model from McPartlon et al. [2022], GVP, and GVP-AF2. Values for GVP and GVP-AF2 are both taken from Hsu et al. [2022]; we take the best reported value for each task across several tested model variants.

For all tasks except DeepSequence, MIF is better than sequence-only methods, and on DeepSequence, adding sequence transfer improves performance above that of the sequence-only methods. Within DeepSequence, MIF-ST beats CARP-640M on 22 out of 41 datasets and MIF on 37 out of 41 datasets. On the other tasks, MIF and MIF-ST achieve similar results, with sequence-transfer not consistently improving zero-shot performance despite improving pretraining performance. Table A2 shows that MIF outperforms CARP-640M on all ten folds tested in the stability dataset, and MIF-ST outperforms

Table 2: Zero-shot effect prediction. We report average Spearman correlation for DeepSequence, Spearman correlation for RBD and GB1, AUROC for MSP, and Pearson correlation for stability.

Regime	Model	Task				
		DeepSequence	MSP	RBD	stability	GB1
sequence	CARP-640M	0.493	0.53	-0.05	0.28	-0.08
	ESM-1b	0.457	-	0.02	-	-
	ESM-1v	0.508	-	0.03	-	-
+structure	Structured Transformer	-	-	-	0.37	-
	GVP	-	0.71	0.60	0.42	-
	GVP+AF2	-	0.71	0.69	0.48	-
	McPartlon et al. [2022]	-	-	-	0.50	-
	MIF	0.402	0.71	0.59	0.45	0.24
	MIF-ST	0.509	0.64	0.55	0.47	0.23

MIF on six out of ten folds. On both MSP and stability, MIF and MIF-ST are comparable to other inverse folding methods, but GVP+AF2 is the clear winner on RBD.

Table 3: AlphaFold structures vs PDB structures.

Model	Spearman ρ			
	MIF		MIF-ST	
	PDB	AF2	PDB	AF2
DeepSequence	0.358	0.407	0.488	0.509
GB1	0.202	0.24	0.199	0.23
RBD	0.59	0.18	0.55	0.18

For DeepSequence, GB1, and RBD, we also compared the effect of using PDB or AlphaFold structures, as shown in Table 3. Surprisingly AlphaFold structures lead to better predictions for both GB1 and DeepSequence. (We were only able to find PDB structures for 38 of the 41 DeepSequence datasets, so the results in Table 3 differ slghtly from those in Table 2. The PDB structures used are listed in Table A1.) As shown in Figure 3a, the AlphaFold structure for GB1 is nearly identical to its PDB structure. It is unclear why AlphaFold structures lead to better zero-shot predictions in these cases. However, using an AlphaFold-multimer prediction for RBD greatly degrades performance. Upon examining the structures, this is not surprising, as AlphaFold places the RBD on the wrong side of ACE2, as shown in Figure 3b.

Table A3 shows zero-shot performance on the GB1 dataset separated by number of mutations using both PDB and AlphaFold structures. Without structural information, CARP-640M performs poorly for even single mutants, and no correlation at all for triple and quadruple mutants. Adding structure allows MIF and MIF-ST to make much better predictions at all mutation levels, but the accuracy nevertheless falls very quickly as the number of mutations increases.

4.2 Out-of-domain generalization

In addition to zero-shot predictions, it is desirable for pretrained protein models to be able to make the types of out-of-domain predictions that often occur in protein engineering campaigns. For example, a protein engineer may want to train a model on single mutants and make predictions for sequences with multiple mutations, or train a model that is accurate for sequences with fitness greater than what is seen in the training set.

We finetune and evaluate on two fitness landscapes:

1. *Rma* NOD: Wu et al. [2019] explore how mutations at seven positions of the *Rhodothermus marinus* (*Rma*) nitric oxide dioxygenase (NOD) enzyme influences enantioselectivity on the reaction of phenyldimethyl silane with ethyl 2-diazopropanoate. We train on 214 variants with mutations at 3 positions and randomly split the variants with mutations at all 7 positions
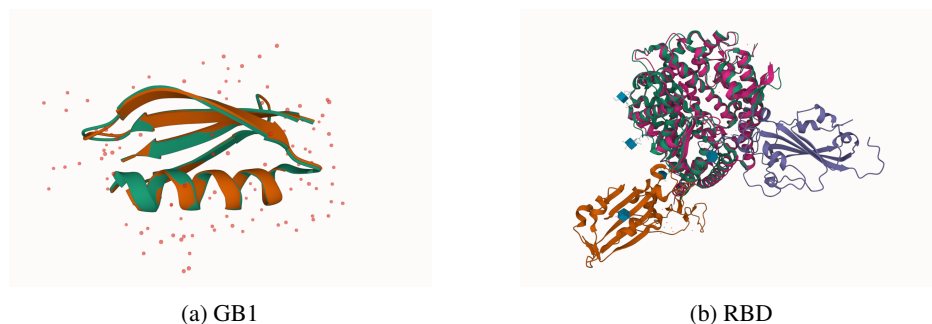
7

(a) GB1

(b) RBD

Figure 3: Comparisons of PDB (blue)and AlphaFold (red) structures for GB1 (PDB:2GI9) and SARS-Cov-2 RBD bound to human ACE2 (PDB:6M0J, orange & grey).

between 40 validation variants and 312 test variants. This tests the model's ability to generalize to mutations at unseen positions based on a small training set. We use PDB 6WK3 as the structure. Measurements were retrieved from ProtaBank [Wang et al., 2018].

2. GB1: We use splits from FLIP [Dallago et al., 2021] over the same GB1 landscape as in Section 4.1. These splits test generalization from fewer to more mutations or from lower-fitness sequences to higher-fitness sequences. We use PDB 2GI9 as the structure.

All models are finetuned end-to-end on a single Nvidia V100 GPU with a 2-layer perceptron as the predictive head until the validation performance stops improving.

Table 4: Out-of-domain prediction of *Rma* NOD enantioselectivity. Uncertainties are standard deviation over 3 random seeds.

Spearman ρ					
CARP-640M		MIF		MIF-ST	
pretrained	naive	pretrained	naive	pretrained	naive
0.69± 0.05	0.70±0.03	0.66±0.11	0.66±0.09	0.77±0.03	0.73±0.05

As shown in Table 4, the MIF-ST architecture outperforms CARP-640M and MIF with and without pretraining on *Rma* NOD. MIF-ST is also the only model for which pretraining improves performance on this task. Table 5 shows results on the GB1 tasks. All models benefit from pretraining on the GB1 tasks. MIF-ST with random weights consistently converged to a degenerate solution where it predicts the same value for all sequences in the test set for all 3 random seeds for 3 of the 4 splits. Combining structure conditioning with sequence transfer seems to help slightly, with the biggest gains coming when the training set is limited to single- and double-mutants. Interestingly, without pretraining, adding structural information does not improve performance.

Table 5: Performance on the FLIP GB1 tasks. Uncertainties are standard deviation over 3 random seeds. Values for CARP-640M are taken from [Anonymous, 2022].

	Model	Spearman ρ			
		1-vs-many	2-vs-many	3-vs-many	low-vs-high
pretrained	CARP-640M	0.19±0.26	0.73±0.03	0.87±0.004	0.43±0.04
	MIF	0.10±0.20	0.71±0.02	0.88±0.004	0.38±0.06
	MIF-ST	0.22±0.03	0.74±0.03	0.88±0.01	0.43±0.01
naive	CARP-640M	0.11±0.07	0.38±0.26	0.68±0.33	0.23±0.26
	MIF	0.03±0.11	0.05±0.12	0.23±0.02	0.17±0.12
	MIF-ST	NaN	NaN	NaN	0.18

8

5   Conclusions

Protein structure is a richer source of information than protein sequence, but the largest protein sequence databases contain billions of sequences, while the number of experimental structures is currently in the hundreds of thousands. In this work, we investigate masked inverse folding on 19 thousand structures and sequences as a pretraining task. We observe that MIF is an effective pretrained model for a variety of downstream protein engineering tasks. We then extend MIF by transferring information from a model trained on tens of millions of protein sequences, improving pretraining perplexity and performance on some downstream tasks. High-quality predicted structures from AlphaFold often improve zero-shot performance over experimental structures. Interestingly, improving pretraining perplexity does not always lead to better downstream performance.

Limitations   However, the MIF and MIF-ST pretraining schemes have several important limitations. First, they require structures as input during downstream tasks. This is ameliorated by the ability to predict high-quality structures for most protein sequences. In this work, we use a single structure for each protein and its variants: we may be able to improve results by predicting structures for all variants. However, this would be computationally expensive for large datasets, and it is currently unclear how good AlphaFold is at predicting the effects of single mutations [Pak et al., 2021]. Some datasets, such as the the FLIP Meltome landscape, contain many unrelated sequences; collating or predicting structures for each sequence would be a significant endeavor. Furthermore, because the structure is held constant during pretraining, it is unclear how to deal with insertions and deletions in downstream tasks. For example, this prevented us from evaluating on the FLIP AAV landscape.

Future work   The related work section suggests improvements that should be composable with MIF and MIF-ST. Using a more advanced GVP or SE(3)-transformer architecture instead of Structured GNN as the base model would likely improve pretraining performance, as would augmenting with AlphaFold structures or adding noise to the input structures. Another obvious extension is to train with an autoregressive or span-masking loss, which should be more amenable to generation tasks, better handle insertions and deletions, and may generalize better to complexes.

Potential negative societal impacts   Machine learning on molecular data generally entails fewer societal risks than work on language, images, medical, or human data. Pretraining data comes from large, curated protein databases that compile results from the scientific literature, with no privacy concerns. However, large pretrained models incur significant energy and monetary costs to train. CARP-640M and ESM are trained on hundreds of V100s for weeks at a time, contributing to greenhouse gas emissions and putting retraining out of the reach of most academic labs.

Outlook   Most work in protein pretraining has used methods borrowed from natural language processing on amino-acid sequences. However, leveraging information from structure, annotations, and even free text should improve performance. We hope that MIF and MIF-ST will lead to more investigations of multimodal protein pretraining tasks.

Data, code, and model availability

Model code is available at `https://github.com/microsoft/protein-sequence-models`. Pretrained model weights and AlphaFold predictions used in this work are available at `https://doi.org/10.1234/mifst`.

Acknowledgments

References

Jacob Devlin, Ming-Wei Chang, Kenton Lee, and Kristina Toutanova. BERT: Pre-training of deep bidirectional transformers for language understanding. *arXiv*, 2018.

Ashish Vaswani, Noam Shazeer, Niki Parmar, Jakob Uszkoreit, Llion Jones, Aidan N Gomez, Łukasz Kaiser, and Illia Polosukhin. Attention is all you need. In *Advances in Neural Information Processing Systems*, pages 5998–6008, 2017.

UniProt Consortium. UniProt: the universal protein knowledgebase in 2021. *Nucleic Acids Res.*, 49 (D1):D480–D489, January 2021.

Baris E Suzek, Yuqi Wang, Hongzhan Huang, Peter B McGarvey, Cathy H Wu, and UniProt Consortium. UniRef clusters: a comprehensive and scalable alternative for improving sequence similarity searches. *Bioinformatics*, 31(6):926–932, 2015.

Martin Steinegger, Milot Mirdita, and Johannes Söding. Protein-level assembly increases protein sequence recovery from metagenomic samples manyfold. *Nature methods*, 16(7):603–606, 2019.

Martin Steinegger and Johannes Söding. Clustering huge protein sequence sets in linear time. *Nature communications*, 9(1):1–8, 2018.

Roshan Rao, Nicholas Bhattacharya, Neil Thomas, Yan Duan, Peter Chen, John Canny, Pieter Abbeel, and Yun Song. Evaluating protein transfer learning with TAPE. In *Advances in Neural Information Processing Systems*, pages 9686–9698, 2019.

Alexander Rives, Joshua Meier, Tom Sercu, Siddharth Goyal, Zeming Lin, Jason Liu, Demi Guo, Myle Ott, C Lawrence Zitnick, Jerry Ma, and Rob Fergus. Biological structure and function emerge from scaling unsupervised learning to 250 million protein sequences. *Proc. Natl. Acad. Sci. U. S. A.*, 118(15), April 2021.

Ratul Chowdhury, Nazim Bouatta, Surojit Biswas, Charlotte Rochereau, George M. Church, Peter K. Sorger, and Mohammed AlQuraishi. Single-sequence protein structure prediction using language models from deep learning. *bioRxiv*, 2021.

Brian L. Hie, Kevin K. Yang, and Peter S. Kim. Evolutionary velocity with protein language models predicts evolutionary dynamics of diverse proteins. *Cell Systems*, 2 2022a. ISSN 24054712. doi: 10.1016/j.cels.2022.01.003.

Brian Hie, Ellen D Zhong, Bonnie Berger, and Bryan Bryson. Learning the language of viral evolution and escape. *Science*, 371(6526):284–288, January 2021.

Joshua Meier, Roshan Rao, Robert Verkuil, Jason Liu, Tom Sercu, and Alexander Rives. Language models enable zero-shot prediction of the effects of mutations on protein function. In M. Ranzato, A. Beygelzimer, K. Nguyen, P.S. Liang, J.W. Vaughan, and Y. Dauphin, editors, *Advances in Neural Information Processing Systems 34*, 2021.

Christian Dallago, Jody Mou, Kadina E Johnston, Bruce Wittmann, Nick Bhattacharya, Samuel Goldman, Ali Madani, and Kevin K Yang. FLIP: Benchmark tasks in fitness landscape inference for proteins. In *Thirty-fifth Conference on Neural Information Processing Systems Datasets and Benchmarks Track (Round 2)*, 2021.

Brian L Hie, Duo Xu, Varun R Shanker, Theodora UJ Bruun, Payton A Weidenbacher, Shaogeng Tang, and Peter S Kim. Efficient evolution of human antibodies from general protein language models and sequence information alone. *bioRxiv*, 2022b.

Felix Teufel, José Juan Almagro Armenteros, Alexander Rosenberg Johansen, Magnús Halldór Gíslason, Silas Irby Pihl, Konstantinos D Tsirigos, Ole Winther, Søren Brunak, Gunnar von Heijne, and Henrik Nielsen. SignalP 6.0 achieves signal peptide prediction across all types using protein language models. *bioRxiv*, 2021.

Vineet Thumuluri, José Juan Almagro Armenteros, Alexander Rosenberg Johansen, Henrik Nielsen, and Ole Winther. DeepLoc 2.0: multi-label subcellular localization prediction using protein language models. *Nucleic Acids Research*, 2022.

John Jumper, Richard Evans, Alexander Pritzel, Tim Green, Michael Figurnov, Olaf Ronneberger, Kathryn Tunyasuvunakool, Russ Bates, Augustin Žídek, Anna Potapenko, et al. Highly accurate protein structure prediction with alphafold. *Nature*, 596(7873):583–589, 2021.

Mihaly Varadi, Stephen Anyango, Mandar Deshpande, Sreenath Nair, Cindy Natassia, Galabina Yordanova, David Yuan, Oana Stroe, Gemma Wood, Agata Laydon, et al. AlphaFold protein structure database: Massively expanding the structural coverage of protein-sequence space with high-accuracy models. *Nucleic acids research*, 50(D1):D439–D444, 2022.

John Ingraham, Vikas Garg, Regina Barzilay, and Tommi Jaakkola. Generative models for graph-based protein design. In *Advances in Neural Information Processing Systems*, pages 15794–15805, 2019.

Alexey Strokach, David Becerra, Carles Corbi-Verge, Albert Perez-Riba, and Philip M Kim. Fast and flexible design of novel proteins using graph neural networks. *bioRxiv*, page 868935, 2020.

Wengong Jin, Jeremy Wohlwend, Regina Barzilay, and Tommi Jaakkola. Iterative refinement graph neural network for antibody sequence-structure co-design. *arXiv preprint arXiv:2110.04624*, 2021.

Bowen Jing, Stephan Eismann, Patricia Suriana, Raphael JL Townshend, and Ron Dror. Learning from protein structure with geometric vector perceptrons. *arXiv preprint arXiv:2009.01411*, 2020.

Matt McPartlon, Ben Lai, and Jinbo Xu. A deep SE (3)-equivariant model for learning inverse protein folding. *bioRxiv*, 2022.

Aaron Chevalier, Daniel-Adriano Silva, Gabriel J. Rocklin, Derrick R. Hicks, Renan Vergara, Patience Murapa, Steffen M. Bernard, Lu Zhang, Kwok ho Lam, Guorui Yao, Christopher D. Bahl, Shin-Ichiro Miyashita, Inna Goreshnik, James T. Fuller, Merika Treants Koday, Cody M Jenkins, Tom Colvin, Lauren P. Carter, Alan J Bohn, Cassie M. Bryan, Daniel Alejandro Fernández-Velasco, Lance J. Stewart, Min Dong, Xuhui Huang, Rongsheng Jin, Ian A. Wilson, Deborah Heydenburg Fuller, and David Baker. Massively parallel de novo protein design for targeted therapeutics. *Nature*, 550:74–79, 2017.

Alfredo Quijano-Rubio, Hsien-Wei Yeh, Jooyoung Park, Hansol Lee, Robert A. Langan, Scott E. Boyken, Marc J. Lajoie, Longxing Cao, Cameron M. Chow, Marcos C. Miranda, Jimin Wi, Hyo Jeong Hong, Lance J. Stewart, Byung-Ha Oh, and David Baker. De novo design of modular and tunable protein biosensors. *Nature*, 2021.

Justin B. Siegel, Alexandre Zanghellini, Helena M. Lovick, Gert Kiss, Abigail R. Lambert, Jennifer L. St.Clair, Jasmine L. Gallaher, Donald Hilvert, Michael H. Gelb, Barry L. Stoddard, Kendall N. Houk, Forrest E. Michael, and David Baker. Computational design of an enzyme catalyst for a stereoselective bimolecular diels-alder reaction. *Science*, 329:309 – 313, 2010.

James E Lucas and Tanja Kortemme. New computational protein design methods for de novo small molecule binding sites. *PLoS Computational Biology*, 16, 2020.

Patrick Bryant, Gabriele Pozzati, Wensi Zhu, Aditi Shenoy, Petras J. Kundrotas, and Arne Elofsson. Predicting the structure of large protein complexes using alphafold and sequential assembly. *bioRxiv*, 2022.

Peter W Rose, Andreas Prlić, Ali Altunkaya, Chunxiao Bi, Anthony R Bradley, Cole H Christie, Luigi Di Costanzo, Jose M Duarte, Shuchismita Dutta, Zukang Feng, Rachel K Green, David S Goodsell, Brian Hudson, Tara Kalro, Robert Lowe, Ezra Peisach, Christopher Randle, Alexander S Rose, Chenghua Shao, Yi-Ping Tao, Yana Valasatava, Maria Voigt, John D Westbrook, Jesse Woo, Huangwang Yang, Jasmine Y Young, Christine Zardecki, Helen M Berman, and Stephen K Burley. The RCSB protein data bank: integrative view of protein, gene and 3D structural information. *Nucleic Acids Research*, 2016. doi: 10.1093/nar/gkw952.

Anonymous. Convolutions are competitive with transformers for protein sequence pretraining. In *Under review at NeurIPS*, 2022.

Ian Sillitoe, Natalie Dawson, and Christine Orengo. CATH protein domain classification (version 4.2). 4 2019. doi: 10.5522/04/7937330.v1. URL https://rdr.ucl.ac.uk/articles/dataset/CATH_protein_domain_classification_version_4_2_/7937330.

Ali Madani, Bryan McCann, Nikhil Naik, Nitish Shirish Keskar, Namrata Anand, Raphael R Eguchi, Po-Ssu Huang, and Richard Socher. ProGen: Language modeling for protein generation. *arXiv*, 2020.

Ali Madani, Ben Krause, Eric R Greene, Subu Subramanian, Benjamin P Mohr, James M Holton, Jose Luis Olmos, Caiming Xiong, Zachary Z Sun, Richard Socher, et al. Deep neural language modeling enables functional protein generation across families. *bioRxiv*, 2021.

Jung-Eun Shin, Adam J Riesselman, Aaron W Kollasch, Conor McMahon, Elana Simon, Chris Sander, Aashish Manglik, Andrew C Kruse, and Debora S Marks. Protein design and variant prediction using autoregressive generative models. *Nature communications*, 12(1):1–11, 2021.

Noelia Ferruz, Steffen Schmidt, and Birte Höcker. A deep unsupervised language model for protein design. *bioRxiv*, 2022.

Daniel Hesslow, N. ed. Zanichelli, Pascal Notin, Iacopo Poli, and Debora S. Marks. RITA: a study on scaling up generative protein sequence models. 2022.

Zachary Wu, Kadina E Johnston, Frances H Arnold, and Kevin K Yang. Protein sequence design with deep generative models. *Current opinion in chemical biology*, 65:18–27, 2021.

Ethan C Alley, Grigory Khimulya, Surojit Biswas, Mohammed AlQuraishi, and George M Church. Unified rational protein engineering with sequence-based deep representation learning. *Nat. Methods*, 16(12):1315–1322, December 2019.

Roshan Rao, Joshua Meier, Tom Sercu, Sergey Ovchinnikov, and Alexander Rives. Transformer protein language models are unsupervised structure learners. In *International Conference on Learning Representations*, 2020.

Ahmed Elnaggar, Michael Heinzinger, Christian Dallago, Ghalia Rehawi, Yu Wang, Llion Jones, Tom Gibbs, Tamas Feher, Christoph Angerer, Martin Steinegger, Debsindhu Bhowmik, and Burkhard Rost. ProtTrans: Towards cracking the language of life's code through Self-Supervised learning. May 2021.

Nadav Brandes, Dan Ofer, Yam Peleg, Nadav Rappoport, and Michal Linial. ProteinBERT: A universal deep-learning model of protein sequence and function. *bioRxiv*, 2021.

Roshan M Rao, Jason Liu, Robert Verkuil, Joshua Meier, John Canny, Pieter Abbeel, Tom Sercu, and Alexander Rives. Msa transformer. In Marina Meila and Tong Zhang, editors, *Proceedings of the 38th International Conference on Machine Learning*, volume 139 of *Proceedings of Machine Learning Research*, pages 8844–8856. PMLR, 18–24 Jul 2021. URL https://proceedings.mlr.press/v139/rao21a.html.

Bassil I Dahiyat and Stephen L Mayo. De novo protein design: fully automated sequence selection. *Science*, 278(5335):82–87, 1997.

Arthur G Street and Stephen L Mayo. Computational protein design. *Structure*, 7(5):R105–R109, 1999.

William F DeGrado, Daniel P Raleigh, and Tracey Handel. De novo protein design: what are we learning? *Current Opinion in Structural Biology*, 1(6):984–993, 1991.

Pehr B Harbury, Joseph J Plecs, Bruce Tidor, Tom Alber, and Peter S Kim. High-resolution protein design with backbone freedom. *Science*, 282(5393):1462–1467, 1998.

Rebecca F Alford, Andrew Leaver-Fay, Jeliazko R Jeliazkov, Matthew J O'Meara, Frank P DiMaio, Hahnbeom Park, Maxim V Shapovalov, P Douglas Renfrew, Vikram K Mulligan, Kalli Kappel, et al. The Rosetta all-atom energy function for macromolecular modeling and design. *Journal of chemical theory and computation*, 13(6):3031–3048, 2017.

Jianfu Zhou, Alexandra E Panaitiu, and Gevorg Grigoryan. A general-purpose protein design framework based on mining sequence–structure relationships in known protein structures. *Proceedings of the National Academy of Sciences*, 117(2):1059–1068, 2020.

Michael Jendrusch, Jan O. Korbel, and S. Kashif Sadiq. Alphadesign: A de novo protein design framework based on alphafold. *bioRxiv*, 2021.

Lewis Moffat, Joe G. Greener, and David T. Jones. Using alphafold for rapid and accurate fixed backbone protein design. *bioRxiv*, 2021.

Lewis Moffat, Shaun M. Kandathil, and David T. Jones. Design in the dark: Learning deep generative models for de novo protein design. *bioRxiv*, 2022.

Ivan Anishchenko, Samuel J Pellock, Tamuka M Chidyausiku, Theresa A Ramelot, Sergey Ovchinnikov, Jingzhou Hao, Khushboo Bafna, Christoffer Norn, Alex Kang, Asim K Bera, et al. De novo protein design by deep network hallucination. *Nature*, 600(7889):547–552, 2021.

Christoffer Norn, Basile IM Wicky, David Juergens, Sirui Liu, David Kim, Doug Tischer, Brian Koepnick, Ivan Anishchenko, Foldit Players, David Baker, et al. Protein sequence design by conformational landscape optimization. *Proceedings of the National Academy of Sciences*, 118 (11):e2017228118, 2021.

Jue Wang, Sidney Lisanza, David Juergens, Doug Tischer, Ivan Anishchenko, Minkyung Baek, Joseph L Watson, Jung Ho Chun, Lukas F Milles, Justas Dauparas, et al. Deep learning methods for designing proteins scaffolding functional sites. *bioRxiv*, 2021.

Sergey Ovchinnikov and Po-Ssu Huang. Structure-based protein design with deep learning. *Current opinion in chemical biology*, 65:136–144, 2021.

Chloe Hsu, Robert Verkuil, Jason Liu, Zeming Lin, Brian Hie, Tom Sercu, Adam Lerer, and Alexander Rives. Learning inverse folding from millions of predicted structures. *bioRxiv*, 2022.

Tristan Bepler and Bonnie Berger. Learning protein sequence embeddings using information from structure. In *International Conference on Learning Representations*, 2019.

Sanaa Mansoor, Minkyung Baek, Umesh Madan, and Eric Horvitz. Toward more general embeddings for protein design: Harnessing joint representations of sequence and structure. *bioRxiv*, 2021.

Can Chen, Jingbo Zhou, Fan Wang, Xue Liu, and Dejing Dou. Structure-aware protein self-supervised learning. *ArXiv*, abs/2204.04213, 2022.

Raphael J. L. Townshend, Rishi Bedi, Patricia Suriana, and Ron O. Dror. End-to-end learning on 3d protein structure for interface prediction. In *NeurIPS*, 2019.

Zuobai Zhang, Minghao Xu, Arian Jamasb, Vijil Chenthamarakshan, Aurélie C. Lozano, Payel Das, and Jian Tang. Protein structure representation learning by geometric pretraining. 2022.

Yue Cao, Payel Das, Vijil Chenthamarakshan, Pin-Yu Chen, Igor V. Melnyk, and Yang Shen. Fold2Seq: A joint sequence(1d)-fold(3d) embedding-based generative model for protein design. *Proceedings of machine learning research*, 139:1261–1271, 2021.

Vignesh Ram Somnath, Charlotte Bunne, and Andreas Krause. Multi-scale representation learning on proteins. In *NeurIPS*, 2021.

Fabian B. Fuchs, Daniel E. Worrall, Volker Fischer, and Max Welling. Se(3)-transformers: 3d roto-translation equivariant attention networks. *ArXiv*, abs/2006.10503, 2020.

Zichen Wang, Steven A. Combs, Ryan Brand, Miguel Calvo Rebollar, Panpan Xu, George Price, Nataliya Golovach, Emmanuel Oluwatobi Salawu, Colby Wise, Sri Priya Ponnapalli, and Peter M. Clark. Lm-gvp: an extensible sequence and structure informed deep learning framework for protein property prediction. *Scientific Reports*, 12, 2022.

Adam J Riesselman, John B Ingraham, and Debora S Marks. Deep generative models of genetic variation capture the effects of mutations. *Nature Methods*, 15(10):816–822, 2018.

Milot Mirdita, Konstantin Schütze, Yoshitaka Moriwaki, Lim Heo, Sergey Ovchinnikov, and Martin Steinegger. Colabfold - making protein folding accessible to all. 2021.

Raphael J. L. Townshend, Martin Vögele, Patricia Suriana, Alexander Derry, Alexander S Powers, Yianni Laloudakis, Sidhika Balachandar, Brandon M. Anderson, Stephan Eismann, Risi Kondor, Russ B. Altman, and Ron O. Dror. ATOM3D: Tasks on molecules in three dimensions. *ArXiv*, abs/2012.04035, 2021.

Justina Jankauskaite, Brian Jiménez-García, Justas Dapkūnas, Juan Fernández-Recio, and Iain H. Moal. Skempi 2.0: An updated benchmark of changes in protein-protein binding energy, kinetics and thermodynamics upon mutation. *bioRxiv*, 2018.

Gabriel J Rocklin, Tamuka M Chidyausiku, Inna Goreshnik, Alex Ford, Scott Houliston, Alexander Lemak, Lauren Carter, Rashmi Ravichandran, Vikram K Mulligan, Aaron Chevalier, et al. Global analysis of protein folding using massively parallel design, synthesis, and testing. *Science*, 357 (6347):168–175, 2017. doi: 10.1126/science.aan0693.

Tyler N. Starr, Allison J. Greaney, Sarah K. Hilton, Daniel Ellis, Katharine H. D. Crawford, Adam S. Dingens, Mary Jane Navarro, John E. Bowen, M. Alejandra Tortorici, Alexandra C. Walls, Neil P. King, David Veesler, and Jesse D. Bloom. Deep mutational scanning of sars-cov-2 receptor binding domain reveals constraints on folding and ace2 binding. *Cell*, 182:1295 – 1310.e20, 2020.

Nicholas C Wu, Lei Dai, C Anders Olson, James O Lloyd-Smith, and Ren Sun. Adaptation in protein fitness landscapes is facilitated by indirect paths. *Elife*, 5:e16965, 2016. doi: 10.7554/eLife.16965.

Zachary Wu, S. B. Jennifer Kan, Russell D. Lewis, Bruce J. Wittmann, and Frances H. Arnold. Machine learning-assisted directed protein evolution with combinatorial libraries. *Proceedings of the National Academy of Sciences USA*, 2019.

Connie Y Wang, Paul M Chang, Marie L Ary, Benjamin D Allen, Roberto A Chica, Stephen L Mayo, and Barry D Olafson. Protabank: A repository for protein design and engineering data. *Protein Science*, 27(6):1113–1124, 2018. doi: 10.1002/pro.3406.

Marina A Pak, Karina A Markhieva, Mariia S Novikova, Dmitry S Petrov, Ilya S Vorobyev, Ekaterina S Maksimova, Fyodor A Kondrashov, and Dmitry N Ivankov. Using alphaFold to predict the impact of single mutations on protein stability and function. *BioRxiv*, 2021.

A Appendix

Table A1: Mappings from DeepSequence alignments to PDB structures.

Alignment	PDB	chain_idx	aln_s	aln_e	pdb_s	pdb_e
AMIE_PSEAE_1_b0	2uxy	0	0	341	0	341
B3VI55_LIPSTSTABLE_1_b0	4zfv	1	9	439	0	430
B3VI55_LIPST_1_b0	4zfv	1	9	439	0	430
BG_STRSQ_1_b0	1gnx	0	14	478	0	464
BLAT_ECOLX_1_b0	1s0w	0	0	263	0	263
BRCA1_HUMAN_1_b0	1jm7	0	0	103	0	103
BRCA1_HUMAN_BRCT_1_b0	4u4a	0	21	235	0	214
CALM1_HUMAN_1_b0	3sjq	0	1	148	0	147
DLG4_RAT_2_b0	2xkx	0	0	101	296	397
DYR_ECOLI_1_b0	5uio	0	0	159	1	160
F7YBW7_MESOW_1_b0	5ceg	1	0	103	0	103
FYN_HUMAN_1_b0	3uf4	0	5	66	0	61
GAL4_YEAST_1_b0	3coq	0	7	75	0	68
HG_FLU_1_b0	6mya	4	16	508	0	493
HIS7_YEAST_1_b0	6ezm	0	2	219	0	217
HSP82_YEAST_1_b0	2cg9	0	1	216	0	215
IF1_ECOLI_1_b0	1ah9	0	1	72	0	71
KKA2_KLEPN_1_b0	1nd4	0	9	264	0	255
MK01_HUMAN_1_b0	7opm	0	0	360	2	362
MTH3_HAEAESTABILIZED_1_b0	3ubt	0	0	328	0	328
P84126_THETH_1_b0	1vc4	0	0	254	0	254
PABP_YEAST_1_b0	6r5k	1	0	96	77	173
PA_FLU_1_b0	7nj7	0	0	716	0	716
POLG_HCVJF_1_b0	3fqq	0	32	114	1	83
POL_HV1N5-CA_1_b0	6wap	0	0	231	0	231
PTEN_HUMAN_1_b0	7jvx	0	6	351	0	345
PYP_HALHA_1_b0	4bbv	0	0	125	0	125
RASH_HUMAN_1_b0	4q21	0	0	169	0	169
RL401_YEAST_1_b0	6zqh	1	0	76	0	76
SUMO1_HUMAN_1_b0	1a5r	0	0	101	2	103
TPK1_HUMAN_1_b0	3s4y	0	15	242	0	227
TPMT_HUMAN_1_b0	2h11	0	16	245	0	229
TRPC_SULSO_1_b0	1igs	0	1	248	0	247
TRPC_THEMA_1_b0	1i4n	0	1	252	0	251
TRY2_RAT_1_b0	3fp6	0	0	223	0	233
UBC9_HUMAN_1_b0	2xwu	0	0	158	0	158
UBE4B_MOUSE_1_b0	2kre	0	8	104	4	100
YAP1_HUMAN_1_b0	2ltw	0	0	36	0	36

Table A2: Zero-shot performance on *de novo* miniproteins from Rocklin et al. [2017], broken out by fold.

Fold	Pearson correlation		
	CARP-640M	MIF	MIF-ST
HHH_{138}	0.41	0.46	0.52
HHH_{134}	0.36	0.45	0.48
$HEEH_{872}$	0.23	0.37	0.41
$HEEH_{726}$	0.21	0.26	0.25
$HEEH_{223}$	0.22	0.53	0.56
$HEEH_{779}$	0.50	0.55	0.62
$EEHEE_{1498}$	0.10	0.36	0.32
$EEHEE_{37}$	0.41	0.65	0.68
$EEHEE_{1716}$	0.22	0.60	0.60
$EEHEE_{1702}$	0.03	0.26	0.24

Table A3: Zero-shot Spearman rank correlation on GB1 broken out by number of mutations.

Model	PDB				AF2			
	1	2	3	4	1	2	3	4
CARP-640M	0.19	0.12	-0.01	-0.01	0.19	0.12	-0.01	-0.01
MIF	0.83	0.64	0.42	0.11	0.84	0.66	0.44	0.15
MIF-ST	0.76	0.62	0.41	0.11	0.83	0.67	0.44	0.15